sustainability

MDPI

Article

Climate Risk Assessment Framework in Real Estate: A Focus on Flooding

Shu-Han Wu [1,*], Chun-Lien Chiang [2], Yu-Hung Huang [2], Jung Huang [2], Jung-Hsuan Tsao [2] and Ching-Pin Tung [1]

[1] Department of Bioenvironmental Systems Engineering, National Taiwan University, Taipei 106319, Taiwan; cptung@ntu.edu.tw
[2] Formosa Climate Smart Service Limited, Taipei 104102, Taiwan; charliechiang@climsmart.com.tw (C.-L.C.); yhhuang@climsmart.com.tw (Y.-H.H.); jhuang@climsmart.com.tw (J.H.); jhtsao@climsmart.com.tw (J.-H.T.)
* Correspondence: d09622002@ntu.edu.tw

Abstract: Climate change exacerbates flood hazards, resulting in risks to real estate values that should be considered by long-term investors. Flood risk presents two major financial risks: market risk and credit risk. Market risk refers to potential property value loss, and credit risk increases the likelihood of mortgage defaults. However, methods and comprehensive data for quantifying global real estate flood risks are lacking. To address this problem, this paper proposes two flood risk assessment frameworks: the local-oriented approach (LOA) and global-oriented approach (GOA). Two hazard and three vulnerability assessment methods are also introduced to support these frameworks. The LOA vulnerability estimates of regions with complete records are required to support the GOA. Taiwan was selected as an example for the LOA assessment, and the results were used to estimate vulnerability overseas in GOA assessments. The results of case studies for buildings located in four cities in different countries were compared. The proposed framework enables investors and asset owners to globally quantify climate risks in real estate, even when the available data are incomplete. Users can choose the most appropriate approach on the basis of the available data and their tolerance for uncertainty.

Keywords: climate risk assessment; flood risk; real estate; price fluctuation

check for updates

Citation: Wu, S.-H.; Chiang, C.-L.; Huang, Y.-H.; Huang, J.; Tsao, J.-H.; Tung, C.-P. Climate Risk Assessment Framework in Real Estate: A Focus on Flooding. *Sustainability* **2024**, *16*, 9577. https://doi.org/10.3390/su16219577

Academic Editors: Xander Wang, Johan Sulaeman and David C. Broadstock

Received: 12 September 2024
Revised: 17 October 2024
Accepted: 1 November 2024
Published: 3 November 2024

Copyright: © 2024 by the authors. Licensee MDPI, Basel, Switzerland. This article is an open access article distributed under the terms and conditions of the Creative Commons Attribution (CC BY) license (https://creativecommons.org/licenses/by/4.0/).

1. Introduction

Climate change is a fundamental risk that long-term investors must consider when attempting to build a resilient portfolio. As extreme weather events become more frequent and intense [1,2], climate change is having an increasingly large effect on real estate prices [3–6]. According to Sayce et al. [7], climate-related risk increases will affect commercial real estate investment in terms of income, outgoings, rate of return, and financing type. More research is needed on the link between commercial real estate pricing and climate risk. The Intergovernmental Panel on Climate Change (IPCC) Sixth Assessment Report defines climate risk as an integrated view of hazards, vulnerability, and exposure [1]. Extreme weather events have heightened awareness of climate risks, and this awareness is influencing market dynamics and real estate prices [6,7]. Property prices may eventually rebound [8] only after an initial decline due to an extreme weather event [9,10]. Flood risk is a focal topic of research regarding the impact of climate change on real estate. Climate change will likely increase flood risks [11–13], which affect property prices [14] and directly threaten properties in flood-prone areas. In regions unaccustomed to such events, decreases in property values and liquidity may be prolonged [8].

Studies on flood risk under climate change have focused on flood-prone areas, flooding probability, flood depth variation, and the accuracy of different hydrological models [15–17]. The World Resources Institute (WRI) Aqueduct Floods tool [18] is commonly used for assessing global-scale riverine and coastal flood hazards. Aqueduct Floods includes both Representative Concentration Pathway (RCP) and Shared Socioeconomic

Pathway (SSP) scenarios for simulating the extent and depth of flood hazard in various regions, scenarios, and time periods for various return periods. The estimates cover a wide range of events and have high data resolution (30 × 30 arc seconds, approximately 1 km × 1 km at the equator). Regarding climate scenarios, Hirabayashi et al. [19] used the Coupled Model Intercomparison Project Phase 6 (CMIP6) climate model data to assess potential global flooding extents and return periods; they identified spatial trends similar to those obtained using CMIP5 climate model data but with higher consistency. In addition, statistical models (e.g., difference-in-difference analysis [20]) and economic models (e.g., hedonic price model [21,22]) have been used to explore the effects of flooding on property values. Clayton et al. [8] indicated that economic losses from flooding are primarily due to operational disruptions, repair costs, insurance claim costs, and devaluation of collateral; their assessment methods varied for each research topic. Overall, analyses of climate change flood hazards involve climate models, flood simulation models, and environmental data. The results of analyses of the effects of flooding on property values (i.e., the vulnerability of property values) are closely related to the housing price models that are selected and the building types investigated.

This study explored the repercussions of floods for real estate prices during climate change in terms of two major risks for long-term investors: market risk and credit risk. Market risk refers to the potential loss of property value and represents anticipated devaluation. Bernstein et al. [23] highlighted that investors and property owners are likely to consider the effects of long-term climate risks on asset value. Increased climate risks in an area would reduce the market demand for real estate, reducing rental and investment willingness and thereby affecting the value and liquidity of the area's real estate [24]. According to Clayton et al. [8] and Sayce et al. [7], the increasing frequency and severity of extreme weather events have heightened the public's awareness of climate risks, resulting in a lasting effect on real estate prices in high-risk regions.

The other type of risk, credit risk, is also known as default risk. Real estate is a large-scale industry with high prices, heavily reliant on debt financing. Natural disasters—such as hurricanes, droughts, and flooding—can cause property damage that leads to a decline in real estate values. Researchers have found that property values in high-flood-risk areas tend to decrease following hurricanes [10,25] and particularly in the months following a major flood event [26] and that these decreases can persist for years [25,27]. Such disasters create financial risks by increasing the likelihood of mortgage defaults, payment delays, and property abandonment [28–31]. Moreover, the impact of and recovery from a disaster differs among building types. Fisher and Rutledge [27] found that the effects of climate-related hurricane risks on property values and returns extend beyond physical damage. Five years after a major hurricane, apartment and retail property values had recovered, but the capital returns of office, hotel, and industrial properties continued to experience a cumulative negative effect. From a credit risk perspective, the effect of a flood on property values may persist for several years rather than just the few months after the disaster [32], a fact that warrants attention from long-term investors.

Risk assessments for the effects of climate-change-driven flooding on real estate values involve four key elements: historical flood events, flood control infrastructure, property price data, and relevant research models. First, historical flood events help in understanding meteorological conditions and flooding causality [33]. Second, flood control infrastructure affects a region's flood resilience; inadequate systems may lead to severe flooding, as seen in disasters in Libya (September 2023) and Dubai, United Arab Emirates (April 2024). Considering local flood control infrastructure when establishing a rainfall–flooding relationship enhances accuracy. Third, comprehensive property price records help when analyzing price fluctuations to gauge flooding's impact. Finally, these elements must be integrated in a relevant model for risk assessments.

However, current research methods and case studies are insufficient for completely characterizing these factors used in global flood risk assessments. Although researchers have explored how climate risks affect property values, most studies have focused on a

few extreme events. Moreover, systematic property registrations are only implemented in regions with highly transparent real estate transactions (such as the United Kingdom, the United States, Japan, and Hong Kong) and have not yet become widespread. Therefore, this study addressed how global real estate climate risks can be quantified and assessed in a portfolio when comprehensive data are not available, focusing on flooding, and proposes a risk assessment framework. Section 2.2 discusses two methods for assessing hazards in regions with and without local flood control infrastructure information and estimating the likelihood of flooding during meteorological events (i.e., precipitation). In Section 2.3, three methods are presented for evaluating global vulnerability linking local and global property price fluctuations to enable estimation of global flood risk through local assessments. Section 3 presents the results for practical cases. Section 4 discusses the limitations of the proposed methods and suggests improvements. The results can serve as indicators for climate risk management, assisting in evaluating the relative risk levels of assets in different locations within an investment or financing portfolio, as well as assessing current and future risk variations. It can also be applied to compare the risk levels of various portfolios. Users can select the most appropriate approach for them in accordance with the available data and their tolerance for uncertainty.

2. Materials and Methods

2.1. Research Framework and Study Area

This study referenced the IPCC's definition of climate risk as an integrated view of hazards, vulnerability, and exposure [1]. In this article, risk is defined as the potential property value loss due to flood events. This risk can be expressed as follows:

$$R = H \times V \times E \quad (1)$$

where R is the expected asset value loss; H represents the hazard, which is the annual probability of flooding; V represents vulnerability, which is the percentage change in property value due to a flood whose magnitude corresponds to a specified probability; and E represents exposure, which is the current value of property located in that area. Methods for assessing hazard and vulnerability are discussed in the subsequent text, and hypothetical assets in various countries are used as the exposure for risk estimations. Table 1 presents the assessment frameworks proposed in this study: the local-oriented approach (LOA) and global-oriented approach (GOA).

Table 1. LOA and GOA frameworks for assessing flood risks in real estate.

Assessment Framework	Hazard	Vulnerability	Advantages
LOA	• Climate Factors: Historical weather data from local stations, used to bias-correct outputs from CMIP6 to project future precipitation. • Nonclimate Factors: Local flood-protection infrastructure information and collected data that are manually processed.	A relationship between flood and property values can be established by analyzing historical local housing prices and flood data.	Provides detailed analysis and produces high-resolution results.
GOA	• Climate Factors: Historical remote-sensing weather data, used to bias-correct outputs from CMIP6 to project global future precipitation. • Nonclimate Factors: Global flood-protection infrastructure or standards information.	Using global macroeconomic or housing price indices, the vulnerability results from the LOA can be scaled up for consistent application across various regions.	Simple, fast, and highly applicable despite the lack of global-scale data.

The LOA is a more accurate method focusing on a specific region, whereas the GOA is a global method with broad coverage and general applicability. Although both local and global hazard studies have been performed, vulnerability studies are less common, and even fewer evaluate global risks. To address this gap, the primary goal of this study was to develop the GOA. Taiwan has a comprehensive meteorological monitoring system and frequent precipitation-related disasters and has thus accumulated extensive flood control experience and rich disaster record data. Moreover, the Actual Price Registration system for Taiwanese real estate transactions, implemented in August 2012, has greatly increased the transparency of real estate transaction information. Leveraging these comprehensive data, this study selected Taiwan as an example for the LOA assessment in this study. This assessment was further used as a basis for estimating global vulnerability data in a demonstration of GOA assessments. Example GOA assessments were performed for two hypothetical buildings—one commercial office and one residential building—in each of four locations: Taipei, London, Brussels, and Frankfurt (Table 2). These four geographically diverse cities were selected due to their importance as key real estate investment markets with strong market records, and their status as major international economic centers. Moreover, Europe is the investment focus for Taiwan's large life insurance companies. Taiwan's life insurance company with the largest overseas real estate assets holds properties in these cities, with significant exposure [34,35]. Therefore, this study uses these locations to test and validate the framework's applicability. Potential property value losses due to flooding for each building were estimated.

Table 2. Study area locations expressed in decimal degrees.

City	Taipei, Taiwan	London, United Kingdom	Brussels, Belgium	Frankfurt, Germany
Location	25.033, 121.568	51.505, −0.086	50.857, 4.354	50.107, 8.656

To help financial institutions evaluate climate physical risks, the Financial Supervisory Commission of Taiwan commissioned the Joint Credit Information Center (JCIC) to establish the "Climate Physical Risk Information Integration Platform for the Financial Industry." The "Flood-Induced Reduction Ratio of Real Estate Value" data from this platform were used to demonstrate the LOA vulnerability analysis method. The dataset comprised 3,834,362 items from Taiwan's Actual Price Registration system for the period from 2012 to 2022, and historical flood data. These data were normalized and analyzed using regressions to quantify property value fluctuations caused by floods. The data were further categorized by administrative division and building type to better analyze the effects of floods on property values; excerpts are provided in Table 3. Nearly 40 domestic banks have adopted this dataset, as required by regulations, for climate scenario analyses and stress tests, facilitating the disclosure of climate-related financial risks [36,37]. For the vulnerability assessments, the housing price fluctuations were assumed to be similar in Taiwanese special municipalities and urban areas in the target countries. Similarly, the price fluctuations in nonmunicipal Taiwanese regions were assumed to be comparable to those in nonurban areas in the target countries. Averaged data from all municipalities and non-municipalities in Taiwan were used to estimate losses for urban and rural areas, respectively, in the target countries.

2.2. Hazard Assessment Method

This paper proposes two hazard assessment methods with different scopes of application and data requirements. An overview of the methods is shown in Table 4 and detailed in the following sections. The assessment primarily considers two key factors: precipitation and flood models. In the WRI Aqueduct Method, described in Section 2.2.1, flood probability is estimated directly from the WRI Aqueduct outputs. WRI output maps are based on global watershed information and can be used for both LOA and GOA hazard

assessment. By contrast, the Flood Protection Standard Method (described in Section 2.2.2) includes local flood-protection infrastructure and precipitation or discharge data in its projection. This method is more suitable for the LOA hazard assessment.

Table 3. Excerpted data on real estate losses caused by floods in Taiwan.

County/City	Town/District	Building Type	MIN	Q25	Q50	Q75	MAX
Taipei City	Da'an District	Residential building	0.150	0.168	0.248	0.282	0.352
Taipei City	Zhongshan District	Office commercial building	0.178	0.228	0.245	0.308	0.370
Taichung City	Xitun District	Suite	0.174	0.330	0.353	0.366	0.477
Hualien County	Fenglin Township	Farmhouse	0.197	0.213	0.256	0.365	0.444

Table 4. Comparison of the proposed methods for assessing flood hazards.

Method	Usage	Description	Data Requirements
WRI Aqueduct Method	LOA & GOA	Potential inundation maps produced by WRI Aqueduct Floods are used to estimate the probability of flooding in various scenarios.	• WRI Aqueduct Floods output maps.
Flood Protection Standard Method	LOA	Key flood-protection infrastructure information in the study area is gathered and analyzed with the driving factors of flooding to generate flood probabilities.	• Climate models and precipitation data. • Key flood-protection infrastructure information in the study area. • Geospatial data required for flood models.

2.2.1. WRI Aqueduct Method

If information about the target area's critical flood-protection infrastructure is unavailable, the WRI Aqueduct Floods tool [18] can be used to assess flood risk. WRI Aqueduct Floods Hazard Maps contain global riverine and coastal flood grid data, including the inundation depth in meters for different scenarios, time periods, and return periods. Flood probability is a necessary component in risk assessments; accordingly, this study used WRI Aqueduct Floods Hazard Maps on a grid basis. The flood conditions for various return periods in each grid are employed to precisely calculate each grid's flood probability. The calculation process is illustrated in Figure 1.

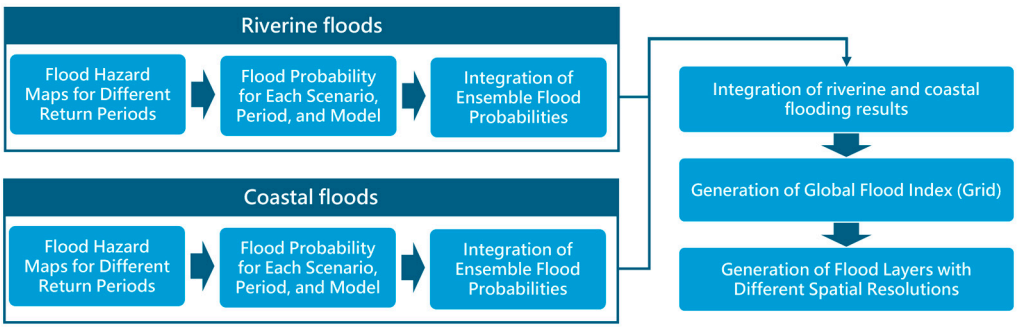


Figure 1. Process for calculating flood probability by using WRI Aqueduct Floods Hazard Maps.

First, hazard maps showing inundation depth in meters for a given scenario and set of assumptions are used to determine whether a flood occurs in each grid cell for the longest analyzed return period. The flood probability is calculated as the reciprocal of the return period at which the inundation depth first occurs. The flood probabilities are then recalculated using different models and assumptions (e.g., sea level rise or land subsidence)

and integrated using an ensemble median method. The maximum flood probability value from riverine and coastal simulations obtained in the previous step is then employed as the flood probability for each grid cell. Additionally, to evaluate the flood risk at the administrative district and national scales, the flood probability of the 99th-percentile grid cell within each administrative district is regarded as the hazard value for that district. The administrative district with the 75th-percentile flood probability within each country is used as the national hazard value; these hazard values are used as global values at these two resolutions.

2.2.2. Flood Protection Standard Method

In the second hazard assessment method, the Flood Protection Standard Method, local infrastructure information is incorporated to improve the accuracy of the flood estimates. An inundation occurs when the net water inflow of an area exceeds the area's flood protection capabilities. The fundamental idea of this method is to calculate flood probabilities on the basis of the flood protection capabilities of the infrastructure for each region and to identify the values of flood-driving factors for various scenarios and periods. Common flood-protection infrastructure includes rainwater sewer systems, flood detention facilities, riverine embankments, and coastal embankments. These designs consider local climate, risk tolerance, and construction costs. They include values representing net water flows in the area, such as rainfall intensity, precipitation, discharge, and return period. While methods for sewer design vary by region, daily rainfall and return periods are broadly applicable. Therefore, to accommodate different cities, this study focuses on daily rainfall for probability analysis. An excerpt of the design return period standards for rainwater sewer systems in administrative regions in Taiwan is listed as examples in Table 5.

Table 5. Excerpted design return period standards for rainwater sewer systems in Taiwan.

City	District	Design Return Period (Year)	Formulation Date
Taipei City	All Districts	5	2004~2005
Taichung City	All Districts	5	1969~1993
Kaohsiung City	All Districts	5	1969
Kaohsiung City	Xiaogang District	5	1989

This assessment method requires determining the flood-protection infrastructure that is critical for drainage in the target area and collecting its design specifications. For areas with incomplete data or unavailable flood control standards, alternative information can be used for estimation. For example, in this study, historical precipitation data and the design return period of the infrastructure were used to estimate the flood protection standard, therefore analyzing the flood probability.

As a case study for evaluating flood hazards in urban areas, London, United Kingdom, was selected. Exact protection standards for London's sewer system are unavailable and were therefore estimated from precipitation data. Therefore, a 30-year return period [38], the uniform standard for newly constructed facilities, was selected for the present estimations. It is important to note that existing flood protection systems in London may have been constructed based on return periods shorter than 30 years. Consequently, using a 30-year return period to assess flood probabilities could underestimate hazard estimates, particularly before the sewer system is fully upgraded to meet this standard. The sewer design date was assumed to align with the baseline period of the CMIP6 climate model (1995–2014). Precipitation within each administrative area was assumed to be handled by its respective sewer system; potential upstream and downstream capacity constraints and other flood control measures were ignored (e.g., pumping facilities for water removal). Precipitation was then simulated under various climate change scenarios, and the likelihood of flooding was estimated as the probability of precipitation surpassing the design

standards. The calculation process for the Flood Protection Standard Method is illustrated in Figure 2 and explained as follows:

1. Referring to Richardson [39], the Gamma distribution is adopted as the probability distribution basis for daily precipitation, and historical precipitation data are used to validate the precipitation distribution parameters for different regions.
2. The Richardson-type weather generation model is used to simulate daily precipitation for baseline and future periods under the ScenarioMIPs of CMIP6 [40]. According to Chen et al. [41], within the framework of this model, the precipitation state (whether it is a rainy day) is first determined by a first-order Markov chain. If a rainy day is projected, precipitation is stochastically sampled from a Gamma distribution; otherwise, it is set to zero. Each simulation generates more than 100 years of daily precipitation data samples for each region. This iterative process produces a long-term precipitation time series, where the total precipitation aligns with the historical long-term mean, and the distribution of consecutive rainy days is consistent with historical observations.
3. These precipitation projections are used to analyze the annual maximum series (AMS) for the baseline and future time periods under different warming projection scenarios.
4. The design return periods of sewer systems in each assessing region are collated.
5. By applying the return period r, the corresponding quantile in the baseline AMS sample can be calculated to determine the precipitation threshold for a flood event. The calculation is as follows:

$$P^* = F_B^{-1}\left(1 - \frac{1}{r}\right) \quad (2)$$

   where ${F_B}^{-1}$ is the AMS quantile function for the baseline period, P^* is the design daily precipitation threshold of sewer system, and r is the design return period of sewer system.
6. The daily precipitation threshold P^* obtained in step 5 is employed to estimate its corresponding quantile $F_P(P^*)$ in the AMS samples for each warming projection scenario (where F_P is the cumulative distribution function of the AMS in the warming projection scenario) to determine the probability of a flood event in each warming scenario.

2.3. Vulnerability Assessment Method

Potential property value losses due to flood events are associated with several factors, including sensitivity to house price fluctuations, building type, and area category (e.g., urban or rural area). Collecting global historical data is challenging; hence, this study proposes three vulnerability assessment methods, described in Table 6, for the GOA assessment. These methods combine comprehensive regional vulnerability analyses with economic and housing price indices to estimate global outcomes. Specifically, the Gross Domestic Product (GDP) Per Capita Adjustment Method (GDPCAM) is detailed in Section 2.3.1, the Integrated Assessment Modelling (IAM) scenario estimation method (IAMSEM) in Section 2.3.2, and the Housing Price Index Method for Adjustment (HPIMOD) in Section 2.3.3.

2.3.1. GDPCAM

The GDPCAM is based on vulnerability results obtained using the LOA scaled up for consistent application in different regions. The method follows the World Bank's view that more economically developed countries have better infrastructure and higher adaptive resilience, potentially resulting in lower economic losses from adverse climate events [42]. According to Fankhauser and McDermott [43], there is a strong and clear relationship between GDP per capita and the impacts of extreme events; however, there is no consensus on how to quantify the extent of this relationship. In their working paper, Fankhauser and McDermott suggest that a 10% increase in a country's GDP per capita reduces economic losses from climate disasters by 3% to 5% [44]. Therefore, the average reduction rate of 4%

was applied in this study. It is notable that this study focuses on proposing an evaluation method and determining the exact reduction rate is beyond its scope. Further research is recommended, and the reduction rate used in this equation can be adjusted as needed for future evaluations. Taiwan was selected as a case study for regional vulnerability analysis. The calculation process for the GDPCAM is illustrated in Figure 3.

Table 6. Comparison of three proposed methods for assessing global flood vulnerability.

Method	Usage	Description	Data Requirements
GDPCAM	GOA	Combines comprehensive regional vulnerability analysis with the GDP per capita in different countries or regions.	GDP per capita in different countries or regions.
IAMSEM		Combines comprehensive regional vulnerability analysis with GDP differences due to floods in different countries or regions as announced by the NGFS.	GDP difference due to floods estimated in IAM scenarios (e.g., analyses released by NGFS).
HPIMOD		Combines comprehensive regional vulnerability analysis with the housing price index in different countries or regions.	Housing price index data (e.g., the OECD National and regional house price indices).

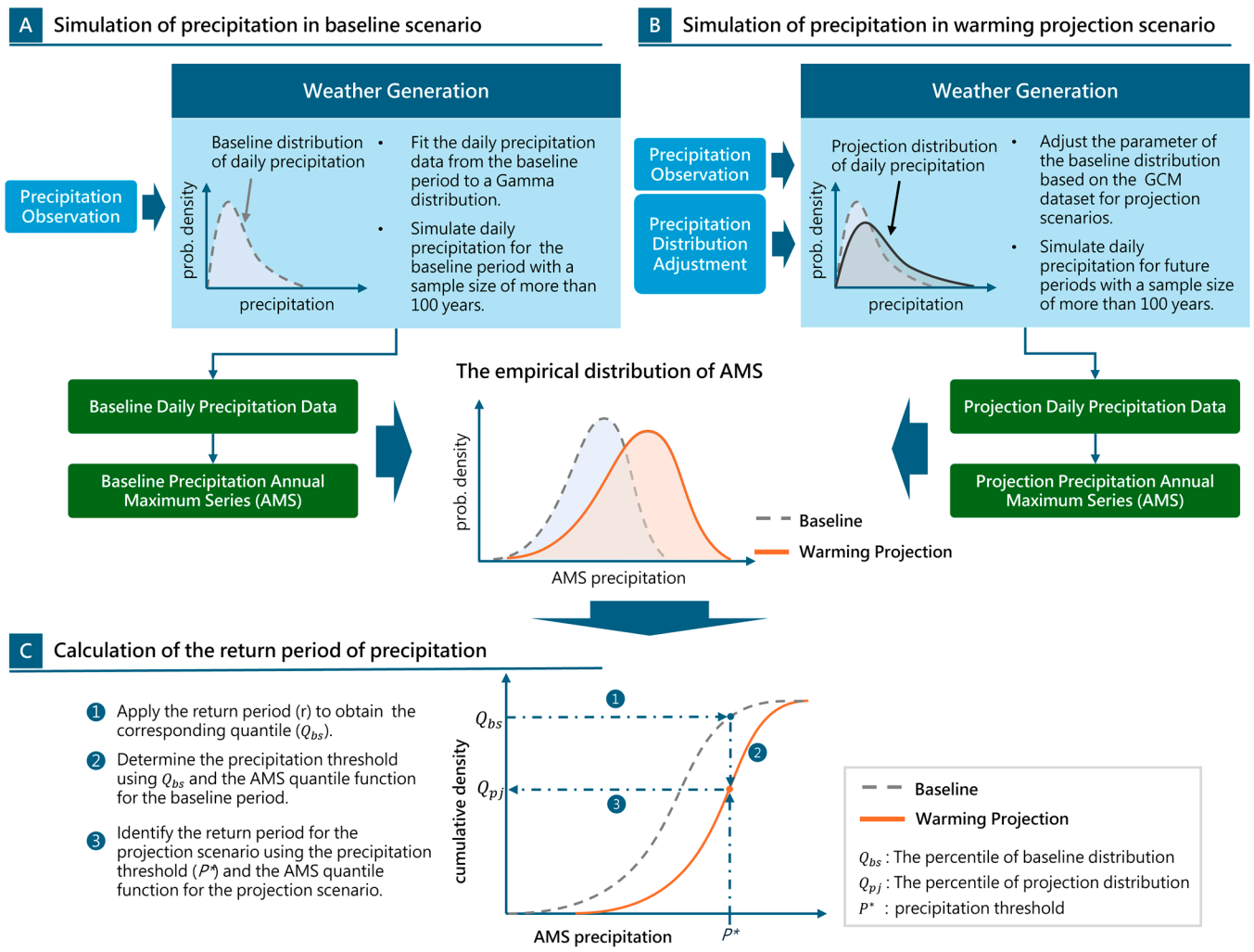


Figure 2. Process for calculating the probability of flooding in the Flood Protection Standard Method.

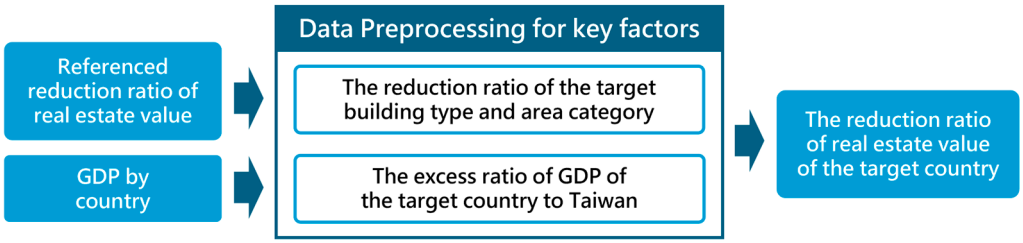


Figure 3. Calculation process for the GDPCAM.

The GDPCAM calculations are as follows:

1. The ratio of the target country's GDP per capita to the benchmark of Taiwan's GDP per capita is calculated.
2. Taiwan's "Flood-Induced Reduction Ratio of Real Estate Value" data are used to select the building type and determine the area category. This helps in estimating the expected property value losses.
3. The expected value losses of the target country can be expressed by Equation (3), based on the percentages provided by Fankhauser and McDermott [44].

$$loss_{TAR} = loss_{REF} \times \left[1 - \left(\left(\frac{GDP_{TAR}}{GDP_{REF}} - 1\right) \times \frac{4\%}{10\%}\right)\right] \quad (3)$$

where $loss_{TAR}$ is the expected housing price impairment value of the target country or region, $loss_{REF}$ is the vulnerability result from LOA, and GDP_{TAR} and GDP_{REF} respectively represent the GDP per capita of the target country or region and the GDP per capita of the LOA region.

This method can be flexibly applied to urban and nonurban areas and for various building types. Compared with the other proposed methods, this approach has the advantages of low data requirements, high accessibility of GDP per capita data, and its simple calculations. It is hence a highly versatile method.

2.3.2. IAMSEM

The IAMSEM combines LOA estimates with IAM simulation results to estimate global vulnerability. IAM combines knowledge from two or more domains into a unified framework. IAM models are a primary tool for conducting integrated assessments. The IAM simulation data employed in this study came from the Network for Greening the Financial System (NGFS) Climate Scenarios dataset, which includes estimates of GDP losses due to floods [45]. The calculation process for the IAMSEM is shown in Figure 4.

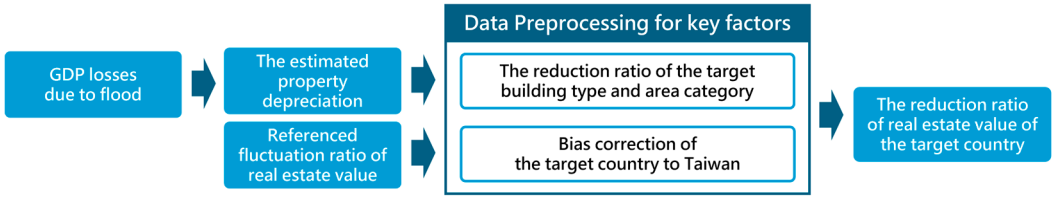


Figure 4. Calculation process for the IAMSEM.

The IAMSEM calculations are as follows:

1. The relationship provided by Williams [46]—which states that for every 1% loss in GDP, property prices drop by 4%—is employed to convert GDP losses due to flood in IAM simulations into property value depreciation.
2. Taiwan's "Flood-Induced Reduction Ratio of Real Estate Value" data are used to select the building type and determine the area category.
3. Assuming that the estimated property depreciation in step 1 follows a similar statistical pattern to the "Flood-Induced Reduction Ratio of Real Estate Value" derived from

historical real estate transaction data in step 2, a relationship between these two datasets is identified and the statistical parameters of the "Flood-Induced Reduction Ratio of Real Estate Value" are estimated for the target area.

4. Assume that the distribution of property value reduction due to flood in the target area exhibits similar fluctuation patterns to those of similar areas in Taiwan. Values published by the JCIC of Taiwan are used, and Equation (4) is employed to adjust the property value reduction due to flood for overseas regions.

$$loss_EST_{TAR} = \left(\frac{loss_{REF} - loss_\mu_{REF}}{loss_\sigma_{REF}} \right) \times loss_EST_\sigma_{TAR} + loss_EST_\mu_{TAR} \quad (4)$$

where $loss_EST_{TAR}$ is the expected housing price impairment value of the target country or region; $loss_{REF}$ is the vulnerability result of a specific building and area condition from LOA; $loss_\mu_{REF}$ is the mean of the vulnerability results from LOA; $loss_\sigma_{REF}$ is the standard deviation of the vulnerability results from LOA; $loss_EST_\sigma_{TAR}$ represents the estimated standard deviation of the expected housing price impairment value of the target region; and loss_EST_μ_{TAR} represents the estimated mean of expected housing price impairment value of the target region.

Because this method uses IAM simulation data to estimate potential losses, it better incorporates the unique influencing factors of each region. However, national-scale data are available for only approximately 50 countries; for the remaining regions, continental or global data could be used as substitutes.

2.3.3. HPIMOD

The HPIMOD adopts the OECD's nominal house price index [47], which includes sales of both newly constructed and existing dwellings with the base year of 2015 and follows the recommendations of the Residential Property Prices Indices manual [48]. This index is then adjusted in accordance with the statistical relationship between Taiwanese and international indices to estimate the vulnerability of global property values. Taiwan's data were obtained from the Sinyi housing price index published quarterly by Sinyi Realty [49]. It is a constant-quality index based on the hedonic pricing method with pooled data that indicate the changes in price of houses sold. A flowchart of the HPIMOD is presented in Figure 5.

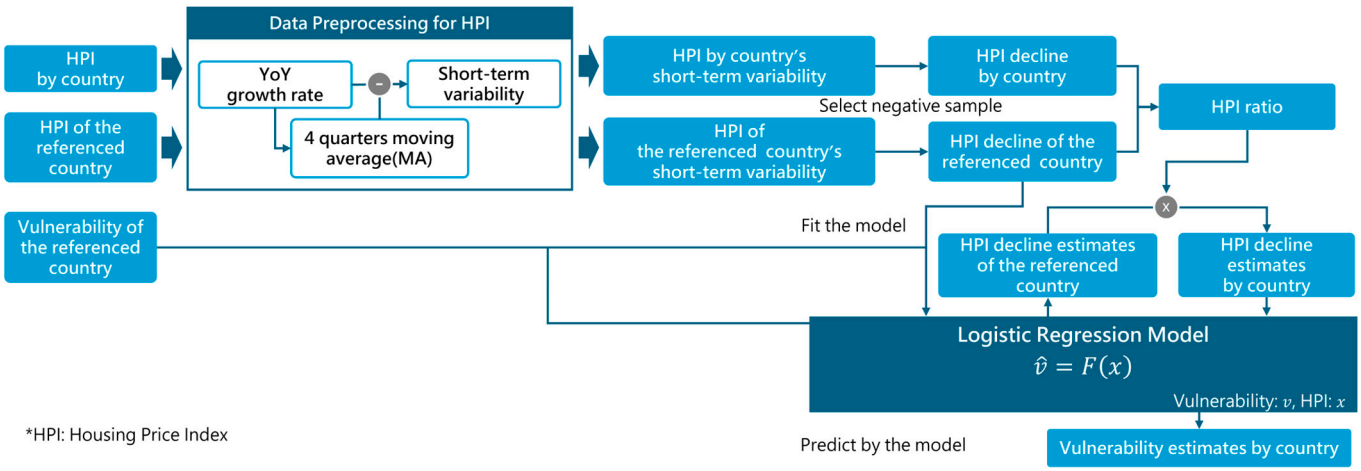


Figure 5. Calculations in the HPIMOD.

Preprocessing for the Housing Price Index

1. Calculate the year-over-year (YoY) change for each housing price index.

The absolute value of the housing price index is not referenced in this method, and the real estate market is influenced by long-term trends (such as fiscal policy, monetary policy,

economic policy, or other country-specific factors). Thus, the YoY change is calculated to isolate short-term fluctuations from long-term trends.

2. Calculate the moving average (MA)

The MA of each year is used to represent the average price state on a medium-term time scale.

3. Retain short-term fluctuations

The MA is removed to identify short-term price fluctuations. If the MA time series average matches the YoY average, the final average short-term fluctuation would be zero; thus, positive and negative values indicate short-term fluctuations in house prices.

Relation Between the Housing Price Index and Vulnerability

The vulnerability of real estate prices for Taiwan is denoted $\overline{v}^*_{TW}(q)$, in which q is the quantile of vulnerability. A statistical relationship was established between the housing price index and the vulnerability of real estate prices. Declines in the housing price index caused by exogenous economic changes in Taiwan's real estate market were assumed to be positively correlated with the intensity of the climate risk vulnerability shock. In the real estate markets, countries with greater average declines in house price indices are also more vulnerable to climate risks. Therefore, a quantile–quantile plot was used to describe the ordinal statistical relationship between declines in Taiwan's housing price index and its real estate value impairment vulnerability for various building types and locations (urban or nonurban areas). This statistical relationship was then applied to the decline in the housing price index of each country to estimate that country's vulnerability.

For the housing price index in Taiwan and other countries, the change ratio of the index time series was computed. All the samples with a negative change ratio were extracted; these are denoted x_{TW} for Taiwan and x_C for other countries. This value indicates the intensity of the reaction of the real estate market to a negative shock. The vulnerabilities v_{TW} of real estate prices from different administrative districts and different quantiles were pooled. The samples for Taiwan and another country were converted to their order statistics—$x^*_{TW}(q)$, $x^*_C(q)$, and $v^*_{TW}(q)$—to calculate the housing price index decline between the other country and Taiwan. The quantiles of the sample can be expressed by Equation (5).

$$r^*(q) = \frac{x^*_C(q)}{x^*_{TW}(q)}\ ,\ q \in [0,\ 1] \tag{5}$$

Next, logistic regression was performed to fit the relationship between these two order statistics:

$$\hat{v}^*_{TW} = \hat{F}(x^*_{TW}) = \frac{1}{1 + e^{-(\hat{\beta}_{0,TW} + \hat{\beta}_{1,\ TW} x^*_{TW})}} \tag{6}$$

where $\hat{v}^*_{TW} = \hat{F}\left(x^*_{TW}\right)$ is the sample regression function and its inverse function is $\hat{x}^*_{TW} = \hat{F}^{-1}\left(v^*_{TW}\right)$. The regression coefficients $\hat{\beta}_0$ and $\hat{\beta}_1$ can be estimated through the ordinary least squares method. Here, leave-one-out cross-validation was used to evaluate the statistical relationship. The results revealed that the relationship established using logistic regression was stable.

Vulnerability Projection Based on Housing Price Index Decline

The estimated housing price index decline in Taiwan corresponding to the vulnerability of its real estate price was calculated as $\hat{\overline{x}}^*_{TW} = \hat{F}^{-1}(\overline{v}^*_{TW})$; the other country's housing price index decline could then be estimated by $\hat{\overline{x}}^*_C = r(q)\hat{\overline{x}}^*_{TW}$. Finally, from the sample regression function, the final vulnerability estimate of the other country could be calculated as $\hat{\overline{v}}^*_C = \hat{F}\left(\hat{\overline{x}}^*_C\right)$.

2.4. Suggestions on Method Selection

Each assessment method proposed in this study requires specific input data, and higher quality data will typically result in a more accurate output. Figure 6 presents a flowchart for selecting a specific method. The availability of design standards for key flood-protection infrastructure is the key factor in selecting a hazard assessment method (Figure 6a). For vulnerability assessments, the HPIMOD should be selected if historical housing price index data are available. Otherwise, the IAMSEM can be used, but this method is a suboptimal choice because it relies on only flood-specific loss data. Finally, the GDPCAM is an alternative if neither type of data is accessible (Figure 6b).

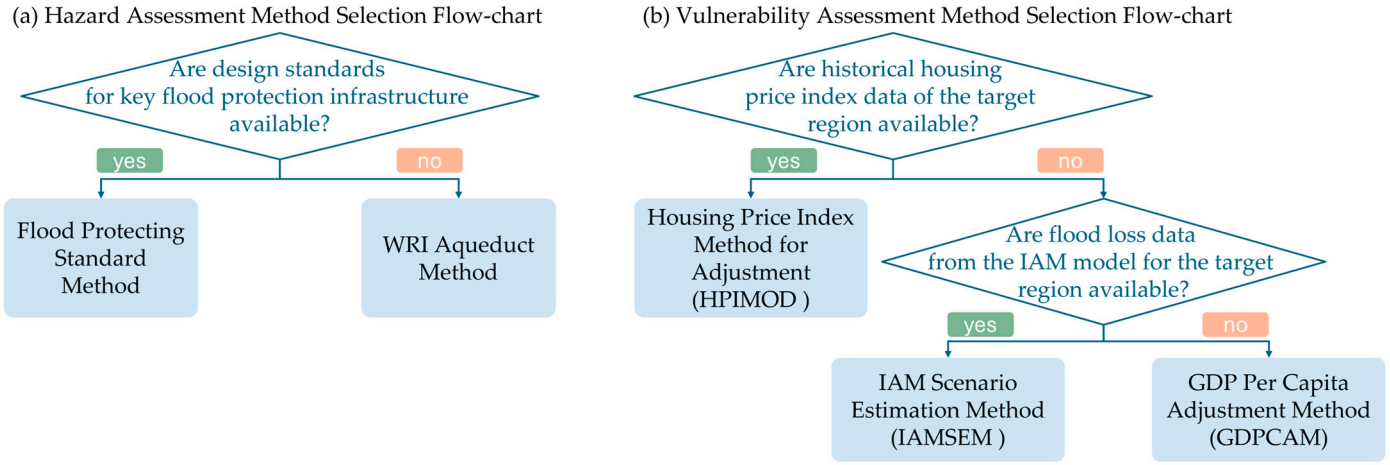


Figure 6. Flowcharts for selecting (**a**) hazard and (**b**) vulnerability assessment methods.

3. Results

3.1. Hazard Assessment Results

3.1.1. Results of the WRI Aqueduct Method

Figure 7 presents the projected spatial distributions of flooding areas under the "Pessimistic" scenario (RCP 8.5, SSP3) when using the WRI Aqueduct Method for the 2080s in the four study areas. This serves as an example to illustrate the results in the four study areas for the 2080s. Blue grid squares represent flooding areas; the background images are layers from ESRI World Imagery [50]. Darker colors indicate areas with a shorter inundation return period and thus a higher inundation probability. For the greater Taipei metropolitan area (Figure 7a), areas projected to have frequent flooding are distributed around the Tamsui River and the Xindian River. In the Greater London Built-up Area (Figure 7b), the flood-prone areas are primarily concentrated along the banks of the River Thames and River Lea. This finding is attributable to the low-lying terrain, urbanization, and hydrological conditions surrounding the rivers. The results for other scenarios have been included in Appendix A for further reference.

3.1.2. Results of the Flood Protection Standard Method

Figure 8 presents the exceedance probability trends for floods under different warming projection scenarios and time periods. In each subplot, the vertical axis on the right is the rainfall return period, and the vertical axis on the left is the probability of the corresponding rainfall return period being exceeded. The solid lines and shading intervals in Figure 7 represent the 50th percentile, 10th percentile, and 90th percentile simulated by all global climate models for each scenario and period. Areas closer to the top of the chart are associated with shorter rainfall return periods, that is, more intense rainfall at shorter intervals.

At the end of the high emission scenario, precipitation events with a 30-year-return-period rainfall intensity are more frequent, increasing to approximately 20-year or even 10-year return periods. Before the middle of the 21st century, the differences between

scenarios are small, however. In Brussels (Figure 8c), the ranges of the 10th and 90th percentiles for different scenarios almost overlap, even until the end of the century. In Frankfurt (Figure 8d), the SSP1-2.6 scenario changes little throughout the century, whereas rainfall frequency clearly increases for higher emission scenarios. In summary, the increase in the return period of rainfall under global warming is not entirely consistent with the emissions in each warming scenario; the results are influenced by discrepancies between global climate models and variations in geographical location and time periods.

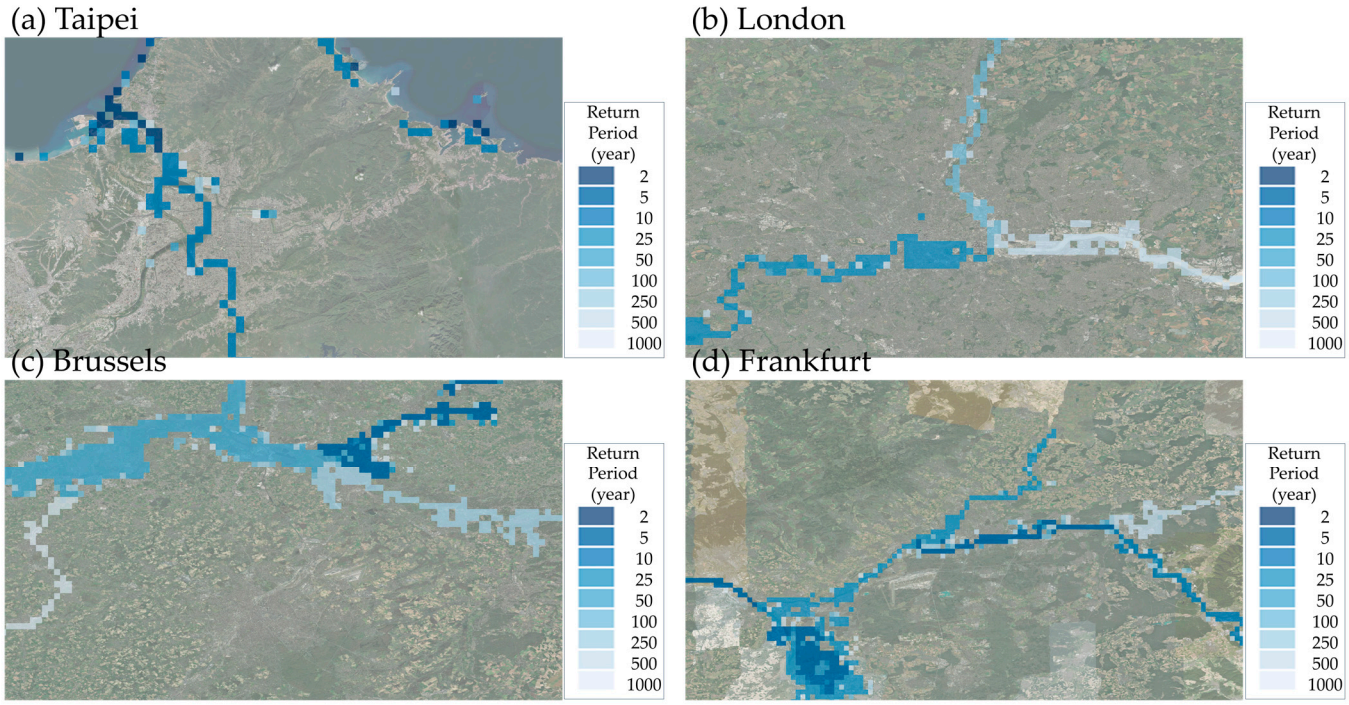


Figure 7. Flooding area spatial distribution in the "Pessimistic" scenario in the 2080s based on the WRI method for (**a**) Taipei, (**b**) London, (**c**) Brussels, and (**d**) Frankfurt.

3.2. Vulnerability Assessment Results

Figure 9 presents the maximum, Q75, median, Q25, and minimum climate vulnerability values of each hypothetical building as assessed using the three proposed methods. The methods are denoted as M1, M2, and M3, respectively, representing the GDPCAM, IAMSEM, and HPIMOD results. MM indicates the mean vulnerability value for all municipalities in Taiwan. For Taipei City (labeled as TPE in Figure 9), the vulnerability estimates represent the mean vulnerability values of the 12 administrative districts in Taipei. The results for the other locations were derived by adjusting the mean vulnerability values of all municipalities (MM) in Taiwan in each of the three methods.

3.3. Risk Assessment Results

The two hazard assessment methods and three vulnerability assessment methods were employed to calculate the climate risk for the study cases. Climate risk was defined as the potential loss in real estate value due to flood and was calculated as the product of the hazard and vulnerability estimates. For the four cities, Tables 7–10, respectively, present the climate risk results under the RCP8.5 scenario in the 2080s, expressed as percentages, of the hypothetical buildings, where these results were obtained using different combinations of hazard and vulnerability methods.

Table 7. Climate risk of the hypothetical buildings in Taipei.

	Hazard Method 1 WRI Aqueduct Method *					**Hazard Method 2 Flood Protection Standard Method**				
	00.00%					**71.25%**				
Climate Risk	Min	Q25	Median	Q75	Max	Min	Q25	Median	Q75	Max
Office Building	0.0%	0.0%	0.0%	0.0%	0.0%	12.3%	15.2%	18.8%	22.1%	25.1%
Residential Building	0.0%	0.0%	0.0%	0.0%	0.0%	10.0%	13.0%	16.7%	22.0%	26.8%

* Hypothetical buildings were in areas with no flooding potential in the WRI Aqueduct flood hazard maps.

Table 8. Climate risk of the hypothetical buildings in London.

	Hazard Method 1 WRI Aqueduct Method					**Hazard Method 2 Flood Protection Standard Method**				
	4.00%					**10.75%**				
Climate Risk	Min	Q25	Median	Q75	Max	Min	Q25	Median	Q75	Max
Office Building										
GDPCAM	0.8%	1.2%	1.8%	2.2%	2.5%	2.0%	3.3%	4.9%	5.9%	6.8%
IAMSEM	0.0%	0.2%	0.4%	0.6%	0.8%	0.0%	0.6%	1.2%	1.7%	2.0%
HPIMOD	1.1%	1.3%	1.8%	2.5%	3.2%	3.0%	3.6%	4.7%	6.6%	8.6%
Residential Building										
GDPCAM	0.6%	1.2%	1.5%	1.9%	2.2%	1.7%	3.1%	4.2%	5.1%	5.9%
IAMSEM	0.0%	0.2%	0.3%	0.5%	0.6%	0.1%	0.5%	0.9%	1.3%	1.6%
HPIMOD	0.9%	1.1%	1.5%	2.1%	2.5%	2.3%	3.1%	3.9%	5.5%	6.8%

Table 9. Climate risk of the hypothetical buildings in Brussels.

	Hazard Method 1 WRI Aqueduct Method *					**Hazard Method 2 Flood Protection Standard Method**				
	00.00%					**14.50%**				
Climate Risk	Min	Q25	Median	Q75	Max	Min	Q25	Median	Q75	Max
Office Building										
GDPCAM	0.0%	0.0%	0.0%	0.0%	0.0%	2.6%	4.2%	6.1%	7.4%	8.5%
IAMSEM	0.0%	0.0%	0.0%	0.0%	0.0%	0.8%	1.9%	3.1%	3.9%	4.6%
HPIMOD	0.0%	0.0%	0.0%	0.0%	0.0%	2.7%	3.0%	3.5%	4.3%	4.5%
Residential Building										
GDPCAM	0.0%	0.0%	0.0%	0.0%	0.0%	2.2%	3.9%	5.2%	6.4%	7.4%
IAMSEM	0.0%	0.0%	0.0%	0.0%	0.0%	0.6%	1.7%	2.5%	3.2%	3.8%
HPIMOD	0.0%	0.0%	0.0%	0.0%	0.0%	2.1%	2.4%	2.7%	3.3%	3.4%

* Hypothetical buildings were in areas with no flooding potential in the WRI Aqueduct flood hazard maps.

Table 10. Climate risk of the hypothetical buildings in Frankfurt.

	Hazard Method 1 WRI Aqueduct Method					**Hazard Method 2 Flood Protection Standard Method**				
	20.00%					**25.25%**				
Climate Risk	Min	Q25	Median	Q75	Max	Min	Q25	Median	Q75	Max
Office Building										
GDPCAM	3.5%	5.8%	8.5%	10.3%	11.9%	4.5%	7.3%	10.7%	13.0%	15.0%
IAMSEM	2.1%	3.8%	5.8%	7.2%	8.3%	2.7%	4.8%	7.3%	9.0%	10.5%
HPIMOD	3.5%	3.8%	4.8%	5.7%	6.2%	4.4%	4.8%	6.0%	7.2%	7.8%
Residential Building										
GDPCAM	3.0%	5.4%	7.2%	8.8%	10.2%	3.8%	6.8%	9.1%	11.1%	12.9%
IAMSEM	1.7%	3.5%	4.9%	6.0%	7.1%	2.2%	4.4%	6.1%	7.6%	8.9%
HPIMOD	2.7%	3.3%	3.7%	4.4%	4.4%	3.4%	4.2%	4.7%	5.6%	5.6%

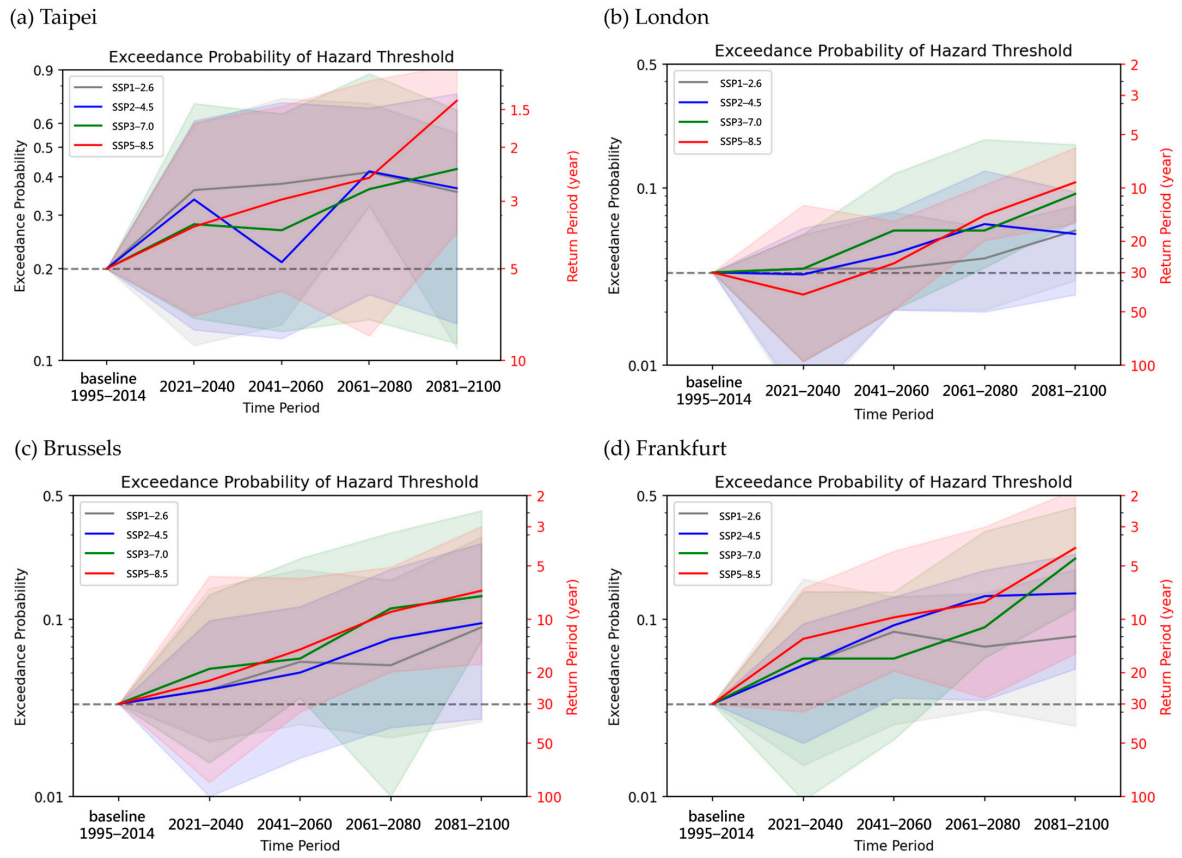


Figure 8. Exceedance probability trends of a flood under different warming projection scenarios and time periods: (**a**) Taipei; (**b**) London; (**c**) Brussels; and (**d**) Frankfurt. The dashed line represents the design return period standard for flood protection infrastructure used in this study: a 5-year return period for Taipei and a 30-year return period for the other locations. The shaded area shows the range between the 5th and 95th percentiles of the multi-model distribution.

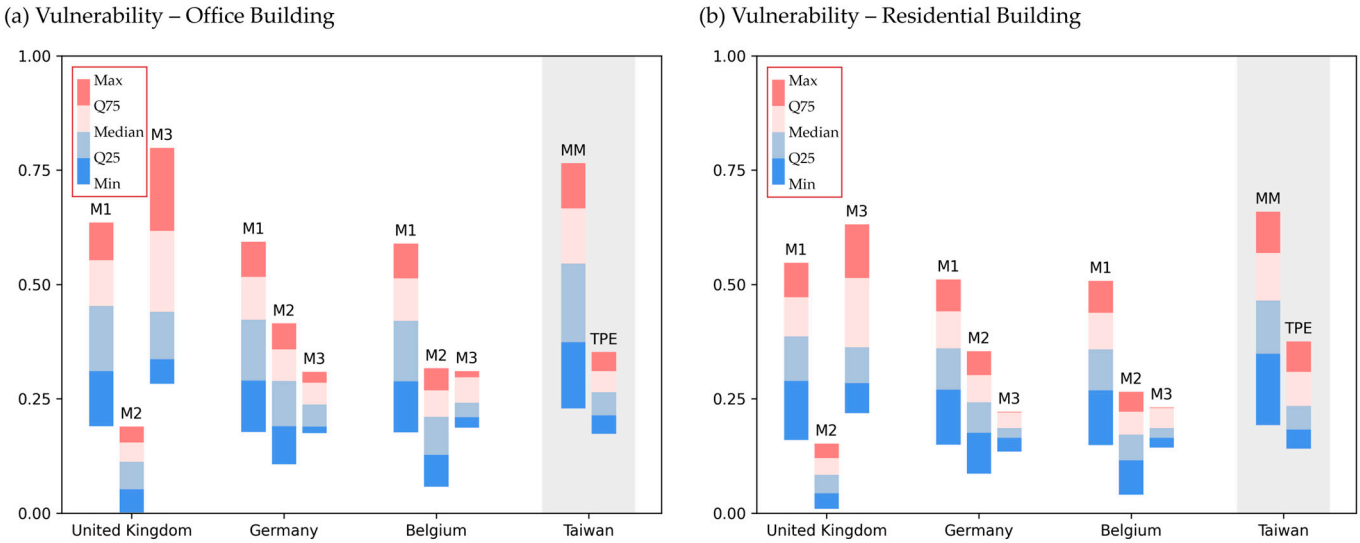


Figure 9. Climate vulnerability of (**a**) commercial office buildings and (**b**) residential buildings, as assessed using the three proposed methods.

4. Discussion

For each city, the climate risk results varied greatly with the method combination. For Taipei (Table 7), the WRI Aqueduct Method estimated a flood hazard probability of zero because the hypothetical buildings are in areas without flooding potential in the WRI Aqueduct flood hazard maps, indicating a deficiency of the WRI Aqueduct Method. The Flood Protection Standard Method, which considers the actual flood control capacity of a site, provides an average flood hazard probability and median climate risk for the commercial office building of 18.8%. This risk is higher than that of the residential building, and the risks for the office building are within a smaller range (12.3–25.1%).

For London (Table 8), the potential flood-induced value losses are less than 9% and 7% for the office building and residential building, respectively. The WRI Aqueduct Method produces a flood hazard probability nearly 2.7 times lower than that of the Flood Protection Standard Method. The GDPCAM and the HPIMOD yield similar vulnerability results, but the estimates of the IAMSEM are clearly lower than those of the other two methods, with risk values between 0.0% and 2.0%.

For Brussels (Table 9), the risk estimates range from 0.0% to 8.5% for the office building and 0.0% to 7.4% for the residential building. As in Taipei, the WRI Aqueduct flood hazard maps classify the locations of the hypothetical buildings in Brussels as having no flooding potential, leading to hazard estimates of zero. The GDPCAM produces the highest summary statistics for vulnerability risk.

Finally, for Frankfurt (Table 10), the climate risk varies from 2.1% to 15.0% for the office building and 1.7% to 12.9% for the residential building. The difference between the two hazard estimates is small. The vulnerability patterns are similar to those obtained for Brussels; the GDPCAM method generates the highest summary statistics for climate risk, and the HPIMOD estimates are within a smaller range.

No consistent correlation between the assessment results of the two hazard methods was discovered. For the WRI Aqueduct Method, the geographical distribution of flooding potential areas in the WRI map was found to lead to differences in flooding probability, which results in a large discrepancy in climate risks between the four cities. Because flooding maps are widely available and frequency analysis calculations are simple, the WRI Aqueduct Method could be easily adopted for regions globally. However, the method has three main limitations. First, it is applicable in limited scenarios and for limited period options. The future flooding simulations from WRI Aqueduct Floods consider only three scenarios (Business as Usual, Optimistic, and Pessimistic) and three periods (2030, 2050, and 2080). Second, the completeness of flood-protection infrastructure data also differs by region. For example, the FLOPROS database [51] used by WRI Aqueduct Floods categorizes Taiwan into simply Taipei and Southern Taiwan, with return periods of 50–200 years and 150 years, respectively; this is an excessive simplification of the actual situation. Third, as the WRI maps currently focus on riverine and coastal floods, this method may therefore be unable to capture flooding situations caused by inadequate urban drainage.

By contrast, the Flood Protection Standard Method provides estimates that better reflect local conditions. In this method, the design standard is used as the threshold for frequency analysis, and the precision and reliability of the method improve as more comprehensive data are collected. However, this method relies on the collection of extensive data and on complex calculations. It requires critical flood-protection infrastructure design standards to be obtained, and their parameters estimated in accordance with the specific characteristics of the location. For example, using river levee design standards as a threshold for riverine flood analysis necessitates the estimation of river flows to calculate flooding probability. Further simulations are necessary to determine the extent, depth, and regions of flooding. In brief, it is recommended for users to understand the main causes of floods and what factors are considered in the assessment. The use of more accurate flood protection standards will enhance the reliability of the assessment results. If information about critical flood-protection infrastructure for the target area is available, the Flood Protection Standard Method may be the better choice of these two hazard assessments.

Regarding the vulnerability assessment methods, the GDPCAM requires the least input data and is highly versatile. However, because this method only uses GDP values coupled with a fixed loss ratio for estimation, the effects of other localized factors on housing prices cannot be considered. The second method, the IAMSEM, also requires little input data. It uses the flood-related losses of each region from NGFS as a key indicator and thus includes influencing factors for each region. However, national-scale data are available for only approximately 50 countries; for the remaining regions, only continental or global data can be used as substitutes. This reliance on the availability of an IAM model for the analyzed region limits the method's applicability. The third method, the HPIMOD, accurately estimates actual fluctuations of local housing prices because it references regional historical housing indices. Its broad applicability stems from accounting for systematic differences in real estate transaction prices across countries, treating these as relative biases between different statistical distributions. By correcting for this variability, the HPIMOD can estimate real estate price fluctuations and vulnerabilities in countries with credible long-term datasets. While it may face limitations in regions where comprehensive housing index data is less available, the method remains highly effective where such data exists. In brief, the selection between these three vulnerability assessment methods depends on data availability and researcher assumptions. The HPIMOD is likely the most accurate method but also has limited applicability.

This study offers a different perspective on flood risk assessment compared to official regional hazard estimates. For instance, the National Science and Technology Center for Disaster Reduction (NCDR) in Taiwan conducted a typhoon-induced flood risk analysis, revealing an average flood probability of 13% for Taipei City under the RCP8.5 scenario between 2075 and 2099 [52], using a dynamic downscaling method focused on typhoon events. In contrast, this study evaluates the probability of rainfall exceeding flood thresholds, providing a broader view of flood risks in the context of climate change. Similarly, the United Kingdom government's estimate shows a flood probability ranging from 0.1% to 1% [53], and Brussel's estimate is approximately 1% [54]. While these figures align with the WRI Aqueduct Method's hazard estimates in this study, they do not account for the impact of climate change. Furthermore, most official flood risk assessments focus on public safety and welfare, with limited discussion of the potential impact on real estate values. Although some researchers have studied the impact of climate risks on property values, most studies have concentrated on extreme events or specific locations, lacking a global-scale assessment method. This research addresses this gap by proposing global-scale risk assessment approaches that specifically focus on the effects of flood events on real estate values under climate change.

5. Conclusions

Climate risk assessment is a critical issue for long-term investors. With the increasing frequency and intensity of extreme weather events, the influence of climate change on real estate prices is significant and cannot be overlooked. Flood risk under climate change is one of the important topics. This paper proposes two risk assessment frameworks for quantifying global real estate climate risks in terms of flood risks: LOA, which focuses on specific regions with high accuracy, and GOA, which achieves global coverage and general applicability. Furthermore, two hazard and three vulnerability assessment methods were developed to support the framework. Case studies were conducted to test and validate the applicability of the framework and compare the proposed assessment methods. Data availability and uncertainty tolerance are the key factors affecting the suitability of each method for assessing hazards and vulnerabilities. By applying these methods, users can estimate the potential asset value loss in their investment or financing portfolios due to floods under climate change. These estimates are useful for managing two major risks for long-term investors: market risk and credit risk. Market risk arises from the devaluation of real estate in areas increasingly exposed to climate risks, reducing demand and investment interest [55]. Credit risk, on the other hand, results from borrowers' potential inability

to service debt due to diminished revenue-generating capacity following flood-related damages. Additionally, the depreciation of properties serving as loan collateral exacerbates the risk of credit losses for lenders [55,56]. The assessment outcomes could act as helpful indicators for climate risk management, enabling users to assess the relative risk levels of assets in various locations and analyze changes in risk over time under climate change scenarios, further formulating strategies to manage and respond to climate risks. These frameworks also provide a way to compare the risk levels of different portfolios. In conclusion, the proposed climate risk assessment framework and methods are expected to provide a solution to support investors and asset owners in their global quantification of climate risks in real estate.

Author Contributions: Conceptualization, S.-H.W., J.H., J.-H.T. and C.-P.T.; Data curation, S.-H.W., C.-L.C., Y.-H.H. and J.H.; Investigation, S.-H.W., C.-L.C., Y.-H.H. and J.H.; Methodology, S.-H.W., C.-L.C., Y.-H.H., J.H., J.-H.T. and C.-P.T.; Project administration, S.-H.W. and J.-H.T.; Resources, J.-H.T. and C.-P.T.; Software, C.-L.C., Y.-H.H. and J.H.; Supervision, S.-H.W., J.-H.T. and C.-P.T.; Visualization, S.-H.W., C.-L.C. and Y.-H.H.; Writing—original draft, S.-H.W., C.-L.C., Y.-H.H. and J.H.; Writing—review & editing, S.-H.W. and Y.-H.H. All authors have read and agreed to the published version of the manuscript.

Funding: This research was funded by the National Science and Technology Council (NSTC) of Taiwan under the project "Study on Environmental SDG Impact Measurement and Management", grant number: NSTC 112-2621-M-002-010-MY2.

Institutional Review Board Statement: Not applicable.

Informed Consent Statement: Not applicable.

Data Availability Statement: The data presented in this study are available on request from the corresponding author. Restrictions apply to the availability of the "Flood-Induced Reduction Ratio of Real Estate Value" data. This data was obtained from the Joint Credit Information Center (JCIC) and are available from the authors with the permission of the JCIC.

Acknowledgments: Special thanks are given to those who participated in the writing of this paper.

Conflicts of Interest: Chun-Lien Chiang, Yu-Hung Huang, Jung Huang, and Jung-Hsuan Tsao are employees of a company. The remaining authors declare that the research was conducted in the absence of any commercial or financial relationships that could be construed as a potential conflict of interest.

Appendix A

Figures A1 and A2 present the projected spatial distributions of flooding areas for the 2080s in the "Business as Usual" and "Optimistic" scenarios, respectively, using the WRI Aqueduct Method in the four study areas.

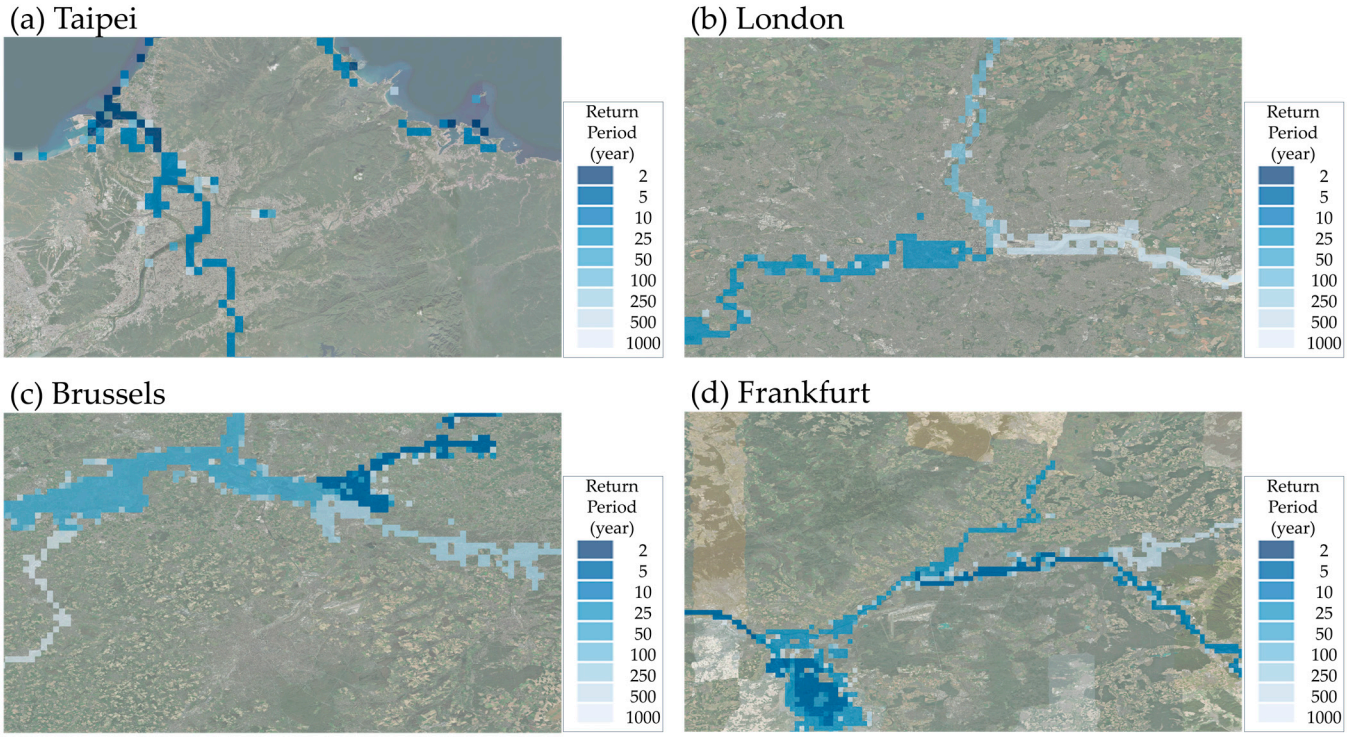


Figure A1. Flooding area spatial distribution in the "Business as Usual" scenario in the 2080s based on the WRI method for (**a**) Taipei, (**b**) London, (**c**) Brussels, and (**d**) Frankfurt.

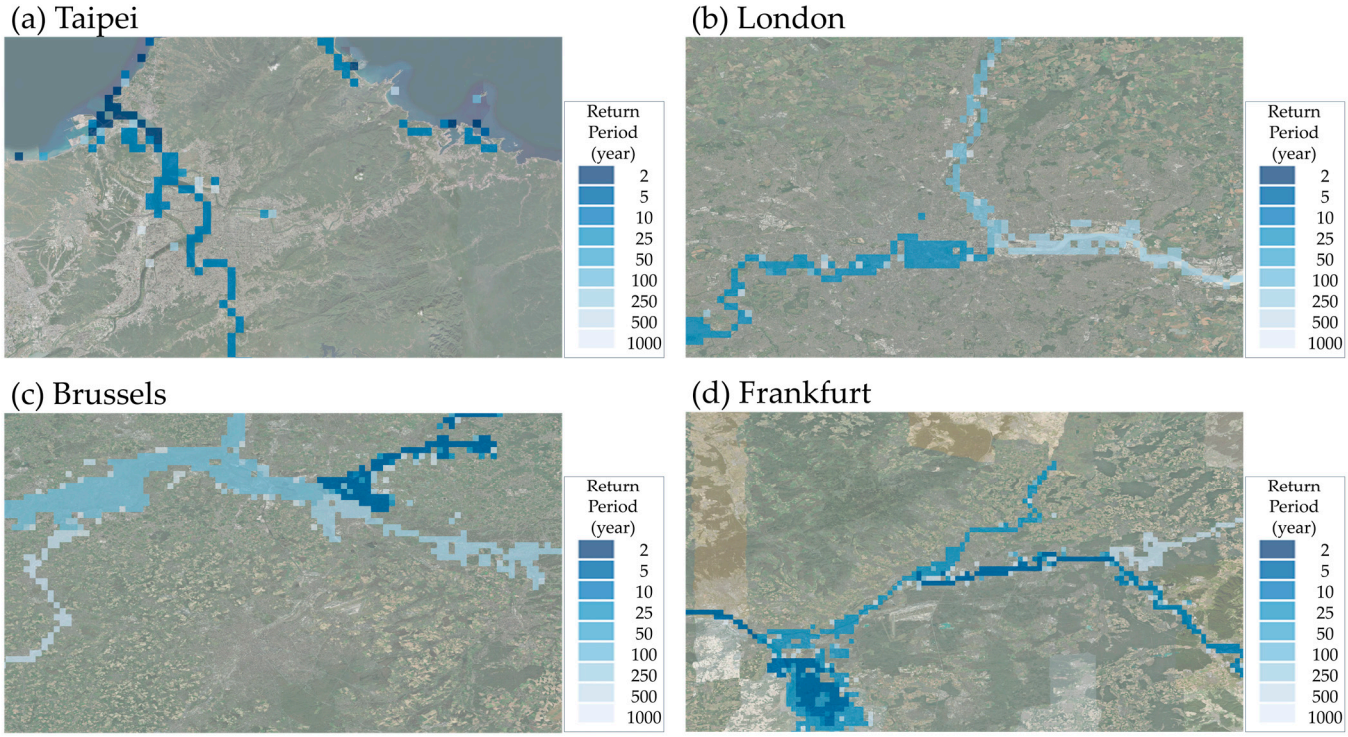


Figure A2. Flooding area spatial distribution in the "Optimistic" scenario in the 2080s based on the WRI method for (**a**) Taipei, (**b**) London, (**c**) Brussels, and (**d**) Frankfurt.

References

1. IPCC. *Climate Change 2023: Synthesis Report. Contribution of Working Groups I, II and III to the Sixth Assessment Report of the Intergovernmental Panel on Climate Change*; IPCC: Geneva, Switzerland, 2023.
2. Yuan, M.; Zhu, Q.; Zhang, J.; Liu, J.; Chen, H.; Peng, C.; Li, P.; Li, M.; Wang, M.; Zhao, P. Global response of terrestrial gross primary productivity to climate extremes. *Sci. Total Environ.* **2021**, *750*, 142337. [CrossRef] [PubMed]
3. Beltrán, A.; Maddison, D.; Elliott, R.J. Is flood risk capitalised into property values? *Ecol. Econ.* **2018**, *146*, 668–685. [CrossRef]
4. Keenan, J.M.; Hill, T.; Gumber, A. Climate gentrification: From theory to empiricism in Miami-Dade County, Florida. *Environ. Res. Lett.* **2018**, *13*, 054001. [CrossRef]
5. Hong, H.; Karolyi, G.A.; Scheinkman, J.A. Climate Finance. *Rev. Financ. Stud.* **2020**, *33*, 1011–1023. [CrossRef]
6. Thompson, J.J.; Wilby, R.L.; Hillier, J.K.; Connell, R.; Saville, G.R. Climate Gentrification: Valuing Perceived Climate Risks in Property Prices. *Ann. Am. Assoc. Geogr.* **2023**, *113*, 1092–1111. [CrossRef]
7. Sayce, S.L.; Clayton, J.; Devaney, S.; van de Wetering, J. Climate risks and their implications for commercial property valuations. *J. Prop. Invest. Financ.* **2022**, *40*, 430–443. [CrossRef]
8. Clayton, J.; Devaney, S.; Sayce, S.; Van de Wetering, J. Climate Risk and Real Estate Prices: What Do We Know? *J. Portf. Manag.* **2021**, *47*, 75–90. [CrossRef]
9. Graham, J.E., Jr.; Hall, W.W., Jr. Hurricanes, housing market activity, and coastal real estate values. *Apprais. J.* **2001**, *69*, 379.
10. Morgan, A. The Impact of Hurricane Ivan on Expected Flood Losses, Perceived Flood Risk, and Property Values. *J. Hous. Res.* **2007**, *16*, 47–60. [CrossRef]
11. Wilby, R.L.; Keenan, R. Adapting to flood risk under climate change. *Prog. Phys.Geogr. Earth Environ.* **2012**, *36*, 348–378. [CrossRef]
12. Field, C.B. *Managing the Risks of Extreme Events and Disasters to Advance Climate Change Adaptation: Special Report of the Intergovernmental Panel on Climate Change*; Cambridge University Press: Cambridge, UK, 2012.
13. Hirabayashi, Y.; Mahendran, R.; Koirala, S.; Konoshima, L.; Yamazaki, D.; Watanabe, S.; Kim, H.; Kanae, S. Global flood risk under climate change. *Nat. Clim. Change* **2013**, *3*, 816–821. [CrossRef]
14. Gibson, M.; Mullins, J.T. Climate Risk and Beliefs in New York Floodplains. *J. Assoc. Environ. Resour. Econ.* **2020**, *7*, 1069–1111. [CrossRef]
15. Meresa, H.; Tischbein, B.; Mekonnen, T. Climate change impact on extreme precipitation and peak flood magnitude and frequency: Observations from CMIP6 and hydrological models. *Nat. Hazards* **2022**, *111*, 2649–2679. [CrossRef]
16. Kimura, Y.; Hirabayashi, Y.; Kita, Y.; Zhou, X.; Yamazaki, D. Methodology for constructing a flood-hazard map for a future climate. *Hydrol. Earth Syst. Sci.* **2023**, *27*, 1627–1644. [CrossRef]
17. Leitão, J.P.; Almeida, M.d.C.; Simões, N.E.; Martins, A. Methodology for qualitative urban flooding risk assessment. *Water Sci. Technol.* **2013**, *68*, 829–838. [CrossRef]
18. Ward, P.J.; Winsemius, H.C.; Kuzma, S.; Bierkens, M.F.P.; Bouwman, A.; De Moel, H.; Loaiza, A.D.; Eilander, D.; Englhardt, J.; Erkens, G.; et al. *Aqueduct Floods Methodology*; World Resources Institute: Washington, DC, USA, 2020; pp. 1–28.
19. Hirabayashi, Y.; Tanoue, M.; Sasaki, O.; Zhou, X.; Yamazaki, D. Global exposure to flooding from the new CMIP6 climate model projections. *Sci. Rep.* **2021**, *11*, 3740. [CrossRef]
20. Zhang, L.; Leonard, T. Flood Hazards Impact on Neighborhood House Prices. *J. Real Estate Financ. Econ.* **2019**, *58*, 656–674. [CrossRef]
21. Beltrán, A.; Maddison, D.; Elliott, R. The impact of flooding on property prices: A repeat-sales approach. *J. Environ. Econ. Manag.* **2019**, *95*, 62–86. [CrossRef]
22. Bin, O.; Kruse, J.B. Real Estate Market Response to Coastal Flood Hazards. *Nat. Hazards Rev.* **2006**, *7*, 137–144. [CrossRef]
23. Bernstein, A.; Gustafson, M.T.; Lewis, R. Disaster on the horizon: The price effect of sea level rise. *J. Financ. Econ.* **2019**, *134*, 253–272. [CrossRef]
24. Roberts, G.; Lafuente, J.; Darviris, T. *Climatic Risk Toolkit: The Impact of Climate Change in the Non-Domestic Real Estate Sector of eight European Countries*; Royal Institution of Chartered Surveyors: London, UK, 2015.
25. Bin, O.; Landry, C.E. Changes in implicit flood risk premiums: Empirical evidence from the housing market. *J. Environ. Econ. Manag.* **2013**, *65*, 361–376. [CrossRef]
26. Belanger, P.; Bourdeau-Brien, M. The impact of flood risk on the price of residential properties: The case of England. *Hous. Stud.* **2018**, *33*, 876–901. [CrossRef]
27. Fisher, J.D.; Rutledge, S.R. The impact of Hurricanes on the value of commercial real estate. *Bus. Econ.* **2021**, *56*, 129–145. [CrossRef]
28. Kousky, C.; Palim, M.; Pan, Y. Flood Damage and Mortgage Credit Risk: A Case Study of Hurricane Harvey. *J. Hous. Res.* **2020**, *29*, S86–S120. [CrossRef]
29. Kousky, C.; Kunreuther, H.; LaCour-Little, M.; Wachter, S. Flood Risk and the U.S. Housing Market. *J. Hous. Res.* **2020**, *29*, S3–S24. [CrossRef]
30. Ataei, H.; Taherkhani, F. Stochastic evaluation of mortgage default losses resulting from flood damages and different mortgage arrangements for post-Katrina Louisiana houses. *Int. J. Hous. Mark. Anal.* **2015**, *8*, 207–222. [CrossRef]
31. Thomson, H.; Zeff, H.B.; Kleiman, R.; Sebastian, A.; Characklis, G.W. Systemic Financial Risk Arising From Residential Flood Losses. *Earth's Future* **2023**, *11*, e2022EF003206. [CrossRef]

32. Ouazad, A.; Kahn, M.E. Mortgage Finance and Climate Change: Securitization Dynamics in the Aftermath of Natural Disasters. *Rev. Financ. Stud.* **2021**, *35*, 3617–3665. [CrossRef]
33. Gil-Guirado, S.; Pérez-Morales, A.; Pino, D.; Peña, J.C.; Martínez, F.L. Flood impact on the Spanish Mediterranean coast since 1960 based on the prevailing synoptic patterns. *Sci. Total Environ.* **2022**, *807*, 150777. [CrossRef]
34. Zhu, H.-l. Fubon Life's Recognition of 6 Billion Losses from German Real Estate Investment Revealed to Be Related to Eurotower. *United Daily News*, 11 April 2024.
35. Wei, Q.-Y.; Huang, H.-L. Three Major Life Insurance Companies Exposed to 65.1 Billion NTD in London Real Estate. *Commercial Times*, 25 June 2016.
36. Li, Y.-J.; Chang, H.-J. A Brief Discussion on Climate Change Scenario Analysis and Stress Testing for Credit Risk in the Banking Industry. *Jt. Credit. Inf. Cent. Mag.* **2023**, *43*, 14–26.
37. Banking Bureau, Financial Supervisory Commission. *Basic Financial Data*; Hsou Yuan CHUANG: New Taipei City, Taiwan, 2024.
38. Mott MacDonald Limited. *London Flooding Review Non-Technical Summary-Stage 3 Report*; Mott MacDonald Limited: Altrincham, UK, 2022.
39. Richardson, C.W. Stochastic simulation of daily precipitation, temperature, and solar radiation. *Water Resour. Res.* **1981**, *17*, 182–190. [CrossRef]
40. Tebaldi, C.; Debeire, K.; Eyring, V.; Fischer, E.; Fyfe, J.; Friedlingstein, P.; Knutti, R.; Lowe, J.; O'Neill, B.; Sanderson, B.; et al. Climate model projections from the Scenario Model Intercomparison Project (ScenarioMIP) of CMIP6. *Earth Syst. Dynam.* **2021**, *12*, 253–293. [CrossRef]
41. Chen, P.-Y.; Tung, C.-P.; Tsao, J.-H.; Chen, C.-J. Assessing Future Rainfall Intensity–Duration–Frequency Characteristics across Taiwan Using the k-Nearest Neighbor Method. *Water* **2021**, *13*, 1521. [CrossRef]
42. World Bank. *Turn Down the Heat: Climate Extremes, Regional Impacts, and the Case for Resilience*; The World Bank: Washington, DC, USA, 2013.
43. Fankhauser, S.; McDermott, T.K.J. Understanding the adaptation deficit: Why are poor countries more vulnerable to climate events than rich countries? *Glob. Environ. Change* **2014**, *27*, 9–18. [CrossRef]
44. Fankhauser, S.; McDermott, T.K.J. *Understanding the Adaptation Deficit: Why are Poor Countries more Vulnerable to Climate Events than Rich Countries?* Centre for Climate Change Economics and Policy Working Paper No. 150, Grantham Research Institute on Climate Change and the Environment Working Paper No. 134. 2013. Available online: https://www.cccep.ac.uk/publication/understanding-the-adaptation-deficit-why-are-poor-countries-more-vulnerable-to-climate-events-than-rich-countries-working-paper-134/ (accessed on 9 October 2024).
45. Richters, O.; Kriegler, E.; Al Khourdajie, A.; Bertram, C.; Bresch, D.N.; Ciullo, A.; Cornforth, E.; Cui, R.; Edmonds, J.; Fuchs, S.; et al. *NGFS Climate Scenarios Data Set (4.1) [Data Set]*; Zenodo: Genève, Switzerland, 2023. [CrossRef]
46. Williams, J.C. Measuring the effects of monetary policy on house prices and the economy. *BIS Paper* **2016**, *88b*, 7–16.
47. OECD. Housing Prices (Indicator). Available online: https://www.oecd.org/en/data/indicators/housing-prices.html (accessed on 3 June 2024).
48. OECD, Eurostat, International Labour Organization, International Monetary Fund, The World Bank and United Nations Economic Commission for Europe. *Handbook on Residential Property Price Indices (RPPIs)*; Eurostat: Luxembourg, 2013. [CrossRef]
49. Chen, P.-F.; Chien, M.-S.; Lee, C.-C. Dynamic modeling of regional house price diffusion in Taiwan. *J. Hous. Econ.* **2011**, *20*, 315–332. [CrossRef]
50. ESRI World Imagery. Available online: https://www.arcgis.com/home/item.html?id=10df2279f9684e4a9f6a7f08febac2a9 (accessed on 2 November 2024).
51. Scussolini, P.; Aerts, J.C.J.H.; Jongman, B.; Bouwer, L.M.; Winsemius, H.C.; de Moel, H.; Ward, P.J. FLOPROS: An evolving global database of flood protection standards. *Nat. Hazards Earth Syst. Sci.* **2016**, *16*, 1049–1061. [CrossRef]
52. National Science and Technology Center for Disaster Reduction (NCDR). Taiwan Climate Change Projection Information and Adaptation Knowledge Platform (TCCIP). Available online: https://tccip.ncdr.nat.gov.tw/ark_fl_impact_eng.aspx (accessed on 15 October 2024).
53. GOV.UK. Check the Long Term Flood Risk for an Area in England. Available online: https://www.gov.uk/check-long-term-flood-risk (accessed on 15 October 2024).
54. Bruxelles Environnement. Inondation aléa et Risque. Available online: https://geodata.leefmilieu.brussels/client/view/1a3cae6b-dd04-4b28-a3e2-c432dc83e24f (accessed on 15 October 2024).
55. Basel Committee on Banking Supervision. *Climate-Related Risk Drivers and Their Transmission Channels*; Bank for International Settlements: Basel, Switzerland, 2021.
56. United Nations Environmental Program Financial Initiative. Managing Physical Climate-Related Risks in Loan Portfolios. Available online: https://www.unepfi.org/themes/climate-change/managing-physical-climate-related-risks-in-loan-portfolios/ (accessed on 28 July 2024).

Disclaimer/Publisher's Note: The statements, opinions and data contained in all publications are solely those of the individual author(s) and contributor(s) and not of MDPI and/or the editor(s). MDPI and/or the editor(s) disclaim responsibility for any injury to people or property resulting from any ideas, methods, instructions or products referred to in the content.